MD Simulation of Crystal Growth from Sodium Chloride Melt

Isao Okada, Toshio Nakashima, Yukio Takahagi, and Junko Habasaki

Department of Electronic Chemistry, Tokyo Institute of Technology at Nagatsuta, Midori-ku, Yokohama 227, Japan

Z. Naturforsch. **50a**, 307–315 (1995); received December 15, 1994

Dedicated to Professor Hitoshi Ohtaki on the occasion of his 60th birthday

Crystal growth on the (100) and (110) faces of sodium chloride from supercooled melt has been studied by molecular dynamics simulation. The growth velocity was considerably higher for the (100) plane (90–100 m/s) than for the (110) plane (transiently 40–50 m/s). Consequently, even from the (110) face, the crystal seems to grow in the [100] direction. Under the present MD conditions, ca. 2 interface layers with a considerable fraction of defects was formed, which means that the surface advances normal to itself without needing steps.

Introduction

Crystal growth from Lennard-Jones liquids [1], liquid silicon [1] and soft-core liquids [2] has intensively been studied by MD simulation, but to our knowledge not that from ionic melts. Therefore, in the present work crystal growth from molten sodium chloride has been studied by an MD simulation.

Method and Model

The basic cell of the MD simulations contained 432 ions. Crystal growth was studied on the (100) and (110) faces of the NaCl crystal. The MD cell is shown in Figure 1. The edge lengths L_x and L_y of the basic cell are given in Table 1. These were based on the crystal density data [3]: $\varrho = 2.1895 - 3.0879 \times 10^{-5}\,(T/\mathrm{K}) - 1.754 \times 10^{-7}\,(T/\mathrm{K})^2$ (g cm^{-3}), the chosen temperature (900 K) and the crystal structure. Periodic boundary conditions were imposed in the x- and y-directions, but not in the z-direction. The ions on the plane $z = 0$ were held fixed at their positions during the whole MD runs. In the z-direction the cells were open to a vacuum; the ions did not "evaporate" even at 2000 K owing to the strong coulombic attractions. Pair potentials obtained by Tosi and Fumi [4] for NaCl crystal were used. The two-dimensional Ewald method [5, 6] was used for the calculation of the coulombic potentials. The 8 nearest replica of the basic cell were considered for the real space calculation. The Gaussian parameter α was taken to be 1.7 L_y. The parameter for the reciprocal space vector $|\boldsymbol{n}|$ was taken up to $\sqrt{2}$. The MD time step was 4 fs. For constant temperature runs, the Woodcock method [7] was used.

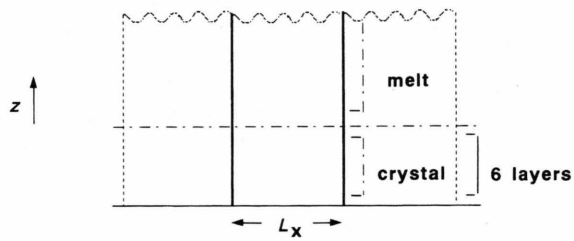

Fig. 1. Model MD cell for the crystal growth.

Table 1. Dimensions of the MD basic cell.

Crystal growth direction	L_x/pm	L_y/pm
[100]	1731	1731
[110]	2449	1731

We distinguished 12 layers, numbered 1, 2, ..., 12.

For (100) the width of the layers up to layer 5 corresponds to the crystal-density at 900 K and amounts to 288 pm. The width of the layers 6 to 11 is 321 pm, and layer 12, ranging above $z = 3225$ pm, holds all the particles not present in the other layers.

For (110) the width of the layers up to layer 11 corresponds to the density of the crystal at 900 K and amounts to 204 pm. Layer 12, ranging above 2142 pm, holds all the particles not present in the other layers.

Reprint requests to Professor I. Okada.

0932-0784 / 95 / 0200-0307 $ 06.00 © – Verlag der Zeitschrift für Naturforschung, D-72027 Tübingen

The MD simulations proceeded in the following way:

(1) In the first stage, the ions in the layers 1–6 were kept at 0 K and the ions in the layers 7–12 were kept at 2000 K for 1000 time steps.

(2) In the second stage, a constant temperature run at $T_0 = 900$ K (experimental m.p.: 1073 K) for the layers 2–12 was performed. This way the interface was equilibrated.

(3) In the third stage, MD runs at constant energy were performed except for layer 1, kept at 0 K, and the layers 2, 3, 11 and 12, kept $T_0 = 900$ K.

The duration of these 3 stages is given in Figure 2.

Crystal growth was studied mainly by comparing relevant properties in the 3rd stage, which was assumed to be in a steady state of growing. As it is often argued that the transfer of the heat of solidification is rate-determining for the crystal growth from melt, the growth of the crystal was performed for constant energy runs rather than for the constant temperature ones.

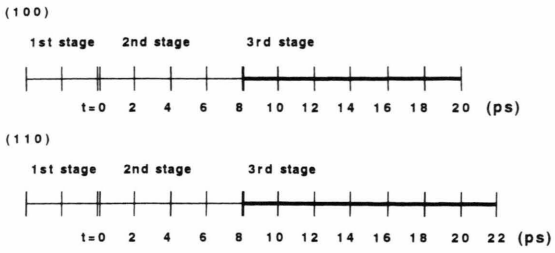

Fig. 2. Timetable of the MD procedure for the (100) and (110) planes.

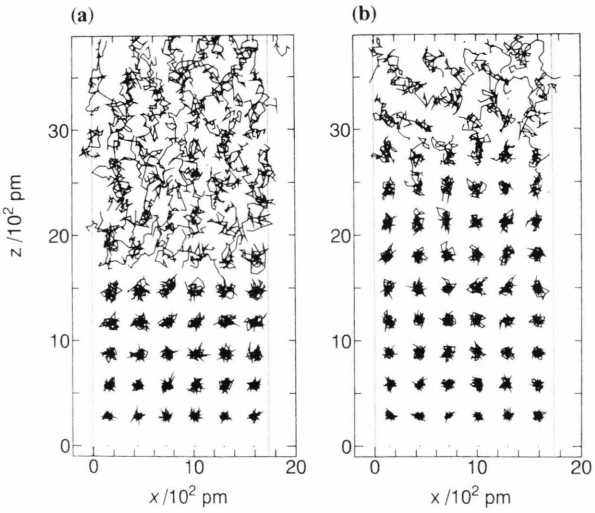

Fig. 3. Trajectories of Na^+ projected on the x-z plane for the (100) case; (a) $t = 8-10$ ps, (b) $t = 18-20$ ps. The thin lines represent the wall of the basic cell.

Results and Discussion

Plots of trajectories of Na^+ projected onto the x-z plane are shown for (100) and (110) in Figs. 3 and 4 respectively. As the trajectories of Cl^- are similar, these are not shown here. In these figures the positions of the ions at every 0.08 ps are connected by solid lines. For (100), the trajectories at $t = 8-10$ ps and 18–20 ps are shown in Figs. (3a) and 3(b), respectively. Evidently, the crystal grows by ca. 3 layers (900 pm) during 10 ps, that is with a velocity of ca. 90 m/s.

Similarly, for (110) the trajectories at 10–12 ps and 20–22 ps are shown in Figs. 4(a) and 4(b), respectively. The velocity of crystallization is 2 layers (400 pm) during 10 ps, that is roughly 40 m/s. In this case, however, the crystal seems to grow in the [100] direction rather than in the [110] direction. The growth in the centre x-axis part of the box was faster, as will be discussed.

The velocity (90 m/s) seems not to be far from reality, as the system is in the supercooled state. For example, the crystallisation velocity of pure metals such as copper has been measured to be as high as 100 m/s [8]. In the MD simulation of argon, the maximum velocity occurs at approximately half the melting point and amounts to 80 m/s [9].

The evolution of the temperature in the layers is shown for (100) and (110) in Figs. 5 and 6, respectively. As mentioned above, the temperatures of the layers 2, 3, 11, and 12 were held at 900 K in the 3rd stage. The increase in temperature is assumed to be caused by the heat of solidification. It is higher for (100) than for (110), and slightly higher in the liquid phase than in the solid phase; the temperature in the 10th layer is near 900 K, as expected as $T = 900$ K for the layers 11 and 12. Although the temperatures in the interfacial region were higher than 900 K, they are still lower than the melting point (1073 K). Therefore, it is not clear whether the generated latent heat accelerated or retarded the solidification. In a preliminary simulation at $T_0 = 1000$ K the crystal did not grow appreciably in the [100] direction during 10 ps.

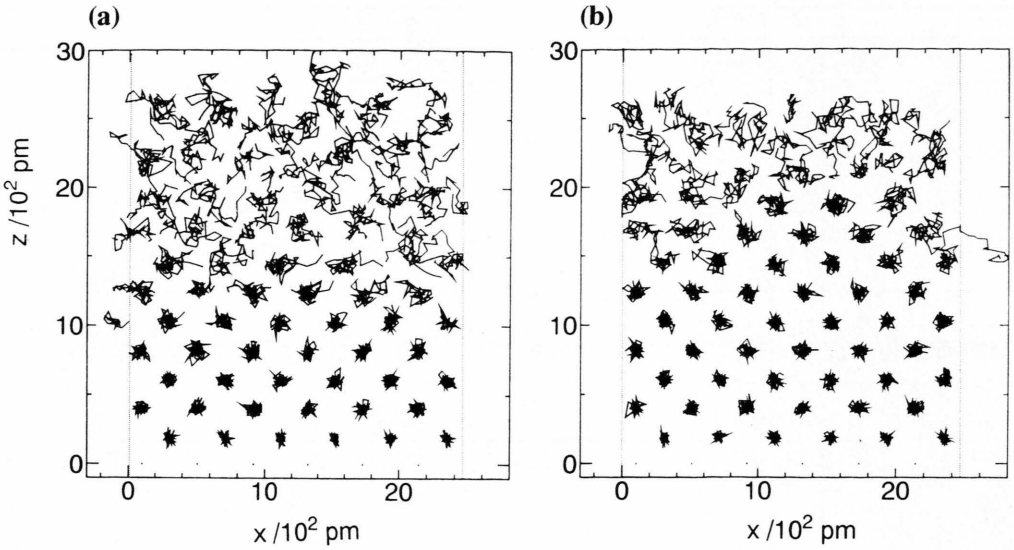

Fig. 4. Trajectories of Na^+ projected on the x-z plane for the (110) case; (a) $t = 10-12$ ps, (b) $t = 20-22$ ps. See also the legend of Figure 3.

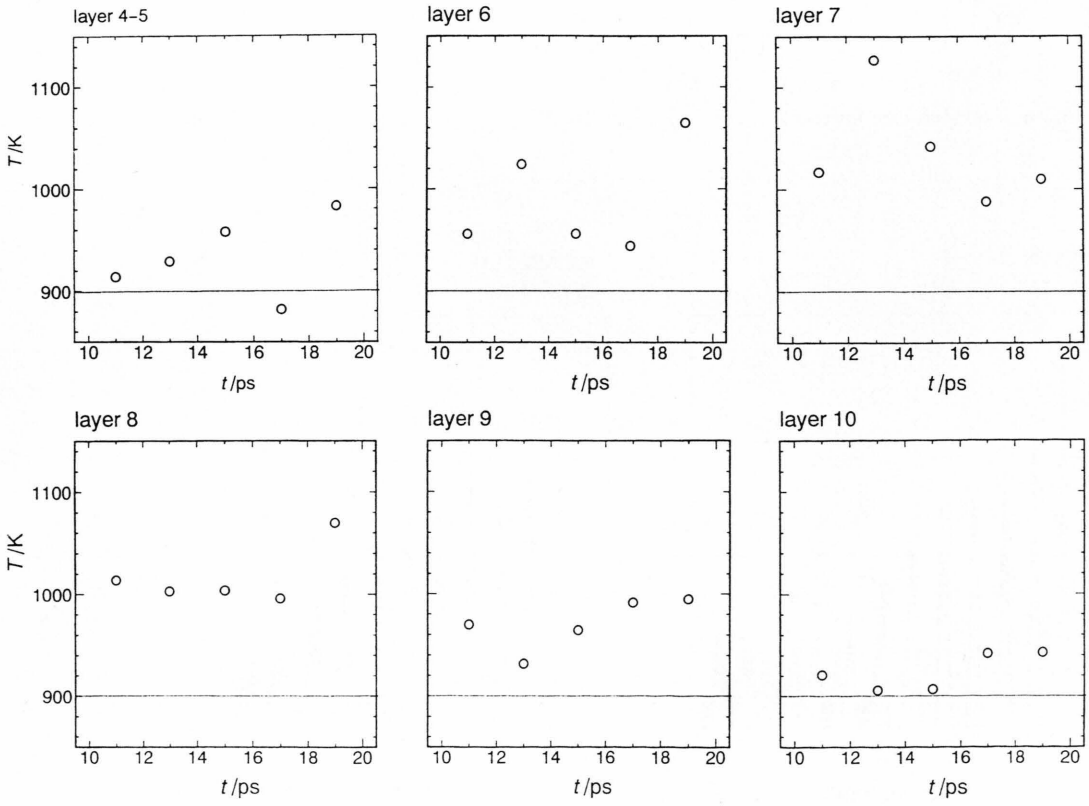

Fig. 5. Evolution of temperature for (100).

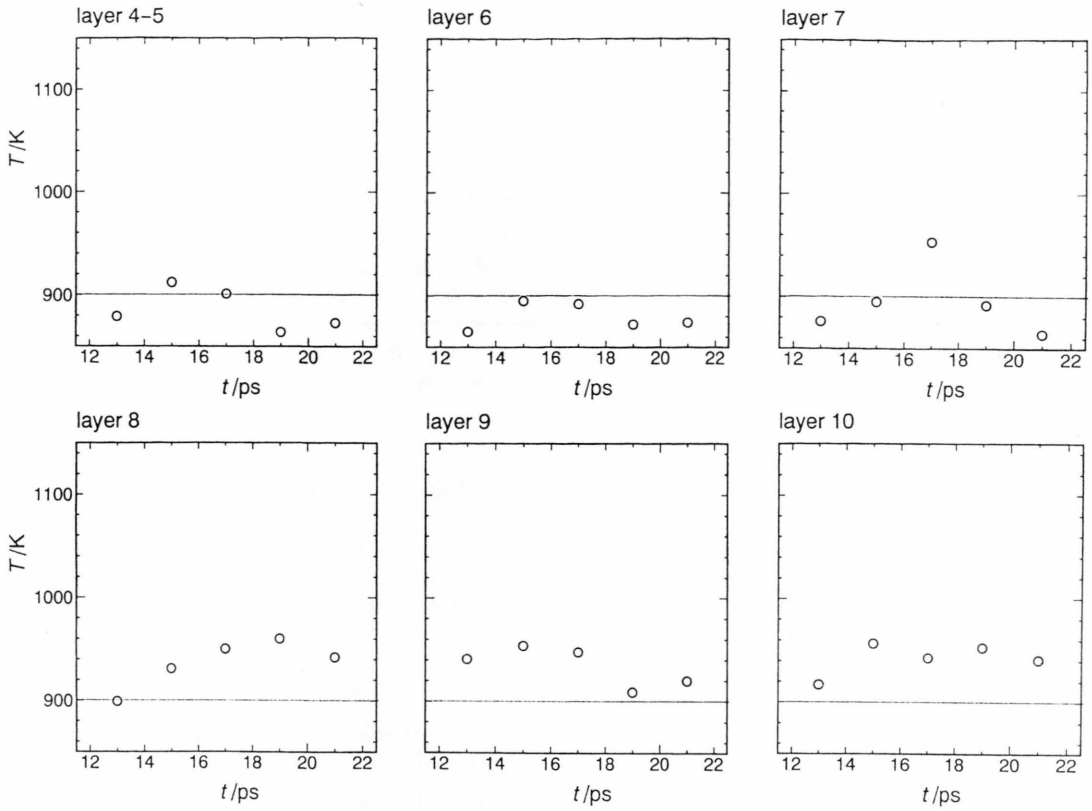

Fig. 6. Evolution of temperature for (110).

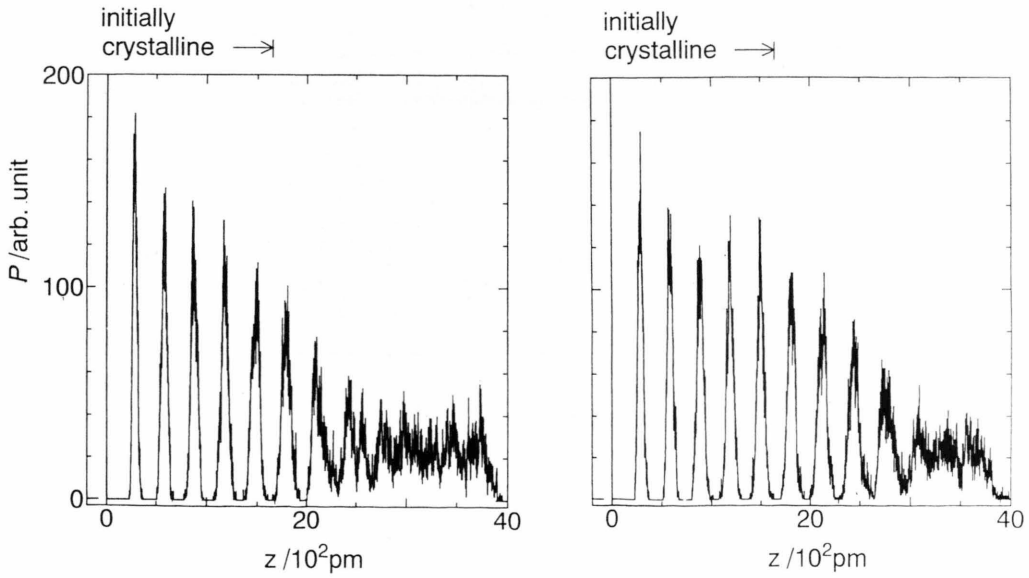

Fig. 7. Density profiles of Na^+ along the z-axis; (a) $t = 12-14$ ps, (b) $t = 18-20$ ps.

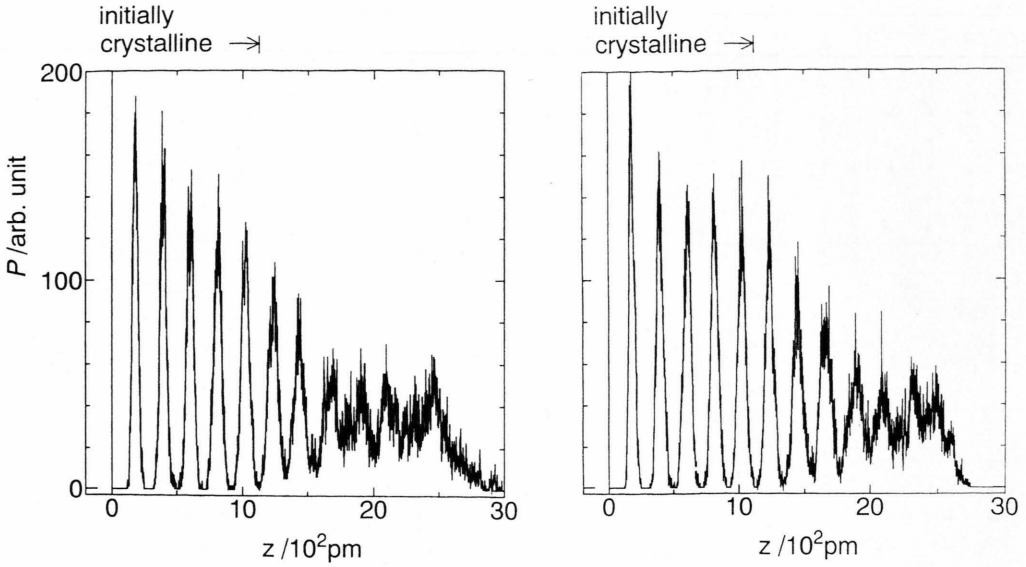

Fig. 8. Density profiles of Na^+ along the z-axis; (a) $t = 12-14$ ps, (b) $t = 20-22$ ps.

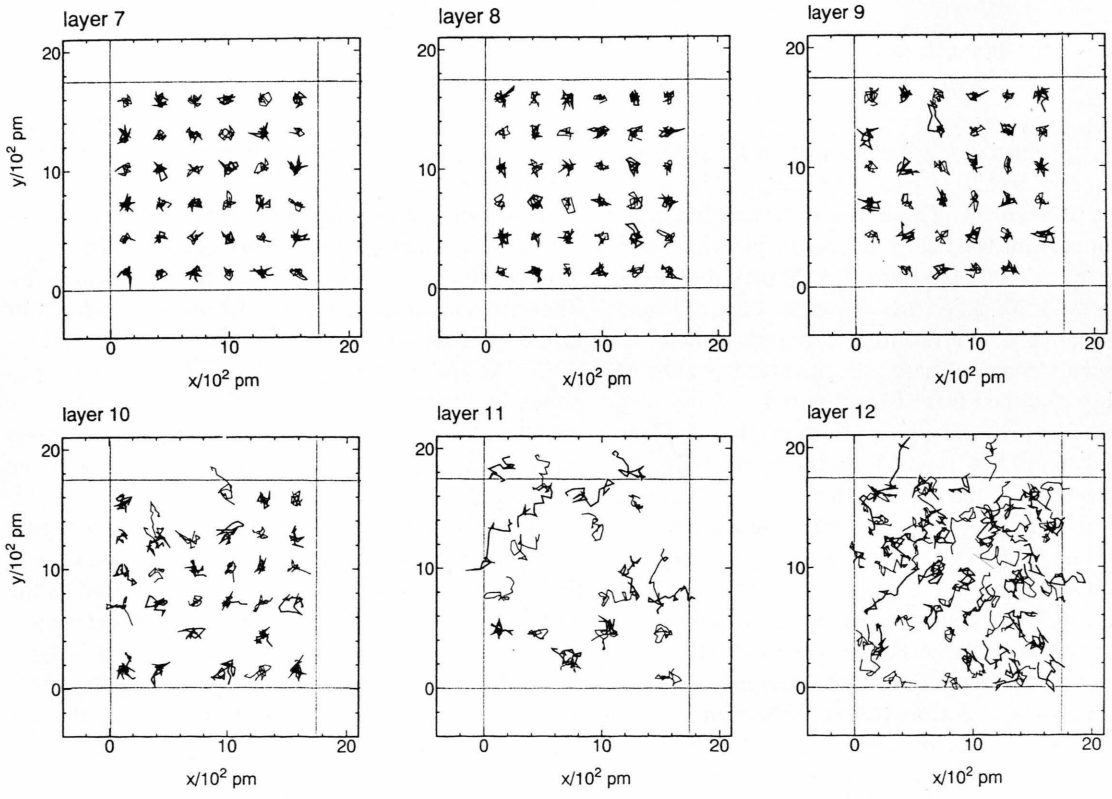

Fig. 9. Na^+ – (bold lines) and Cl^- – (fine lines) trajectories during $t = 18-20$ ps, projected on the x-y plane of (100). The ions were in the indicated layers at $t = 18$ ps.

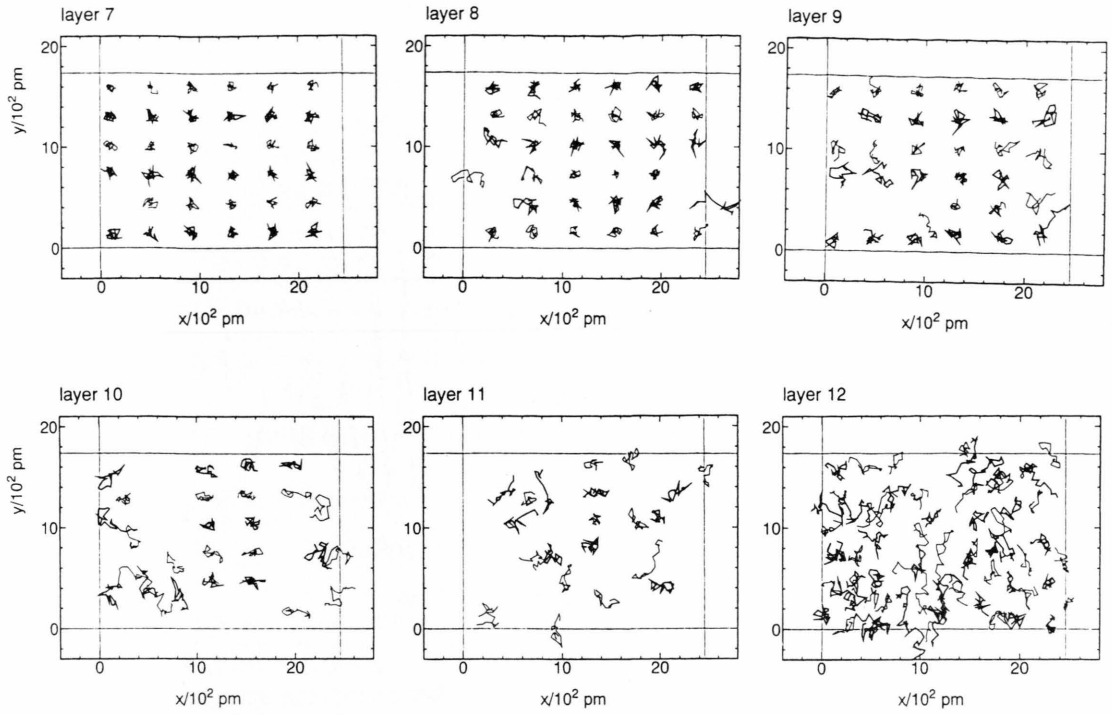

Fig. 10. Na^+ – (bold lines) and Cl^- – (fine lines) trajectories during $t = 20-22$ ps, projected on the x-y plane of (110). The ions were in the indicated layers at $t = 20$ ps.

Density profiles along the z-direction for (100) are shown for Na^+ at 12–14 ps and 18–20 ps in Figs. 7(a) and 7(b), respectively. These figures reveal that crystallisation advances by ca. 2 layers in 6 ps, which corresponds to ca. 100 m/s. For (110), density profiles at 12–14 ps and 20–22 ps are shown in Figs. 8(a) and 8(b), respectively. The resulting apparent growth velocity is ca. 50 m/s. These velocities are consistent with those obtained from Figs. 3 and 4.

Figures 9 and 10 show projections on the x-y plane of the motions of Na^+ and Cl^- in the layers 7–12, the time periods being the same as those in Figs. 3 and 4, respectively. Figure 9 suggests that there are about 2 diffuse layers for (100). Coexistence of regions of crystallinity with regions of defects rather than with those of fluidity within the layer is observed, although the x-y plane area is not large. Figure 9 shows that in (100) the defects in the boundary region become occupied by diffusion of ions mainly in the z-direction.

In the case of (110) (Fig. 10) the crystal grew favourably in the middle x-axis part of the box. This does not necessarily indicate a crystal growth by steps but may rather indicate that the crystal advances more favourably in the [100] direction, as is also suggested by Figure 4.

Some mean square displacements of Na^+ in the x-y plane and z-direction have been calculated. The registered displacements start at $t = 14$ ps and end at 16 ps. They are shown as functions of $t' = r - 14$ ps for four layers of (100) and (110) in Figs. 11 and 12, respectively. As the number of cations in each layer was about 18, the statistics is poor. Further, for (110), the analysis along the layers perpendicular to the z-axis is not so meaningful, as the crystal seems to grow in the [100] direction.

For (100) the displacements in the growth region seem to be more pronounced in the z-direction than in the x-y plane. The ions seem to become ordered by the motion mainly in the z-direction in the diffuse layer, as mentioned above. However, this may perhaps be only caused by the short periodicity in the x-y plane. MD simulations with larger particle numbers in the x-y plane are needed even for (100) to make it clearer.

For an infinite monolayer in a perfect crystal having the inter-ionic distance at 900 K, the configurational energies of Na^+ and Cl^- are calculated to be -6.451

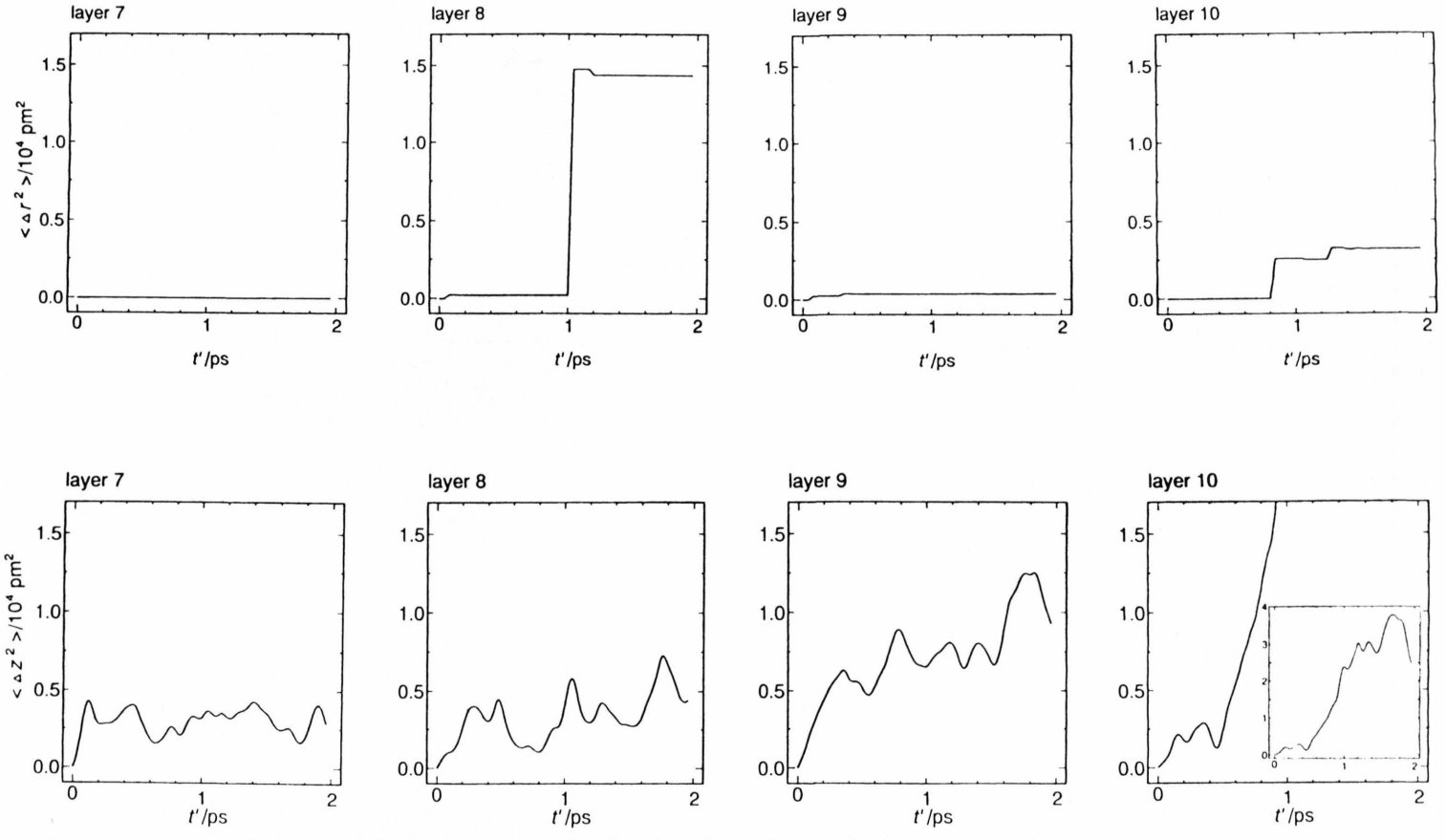

Fig. 11. Mean square displacements in the x-y (upper) and z-directions (lower) for (100) for ions present in the indicated layers at $t = 12$ ps. In the inset of layer 10, the full scale in the z-direction is shown.

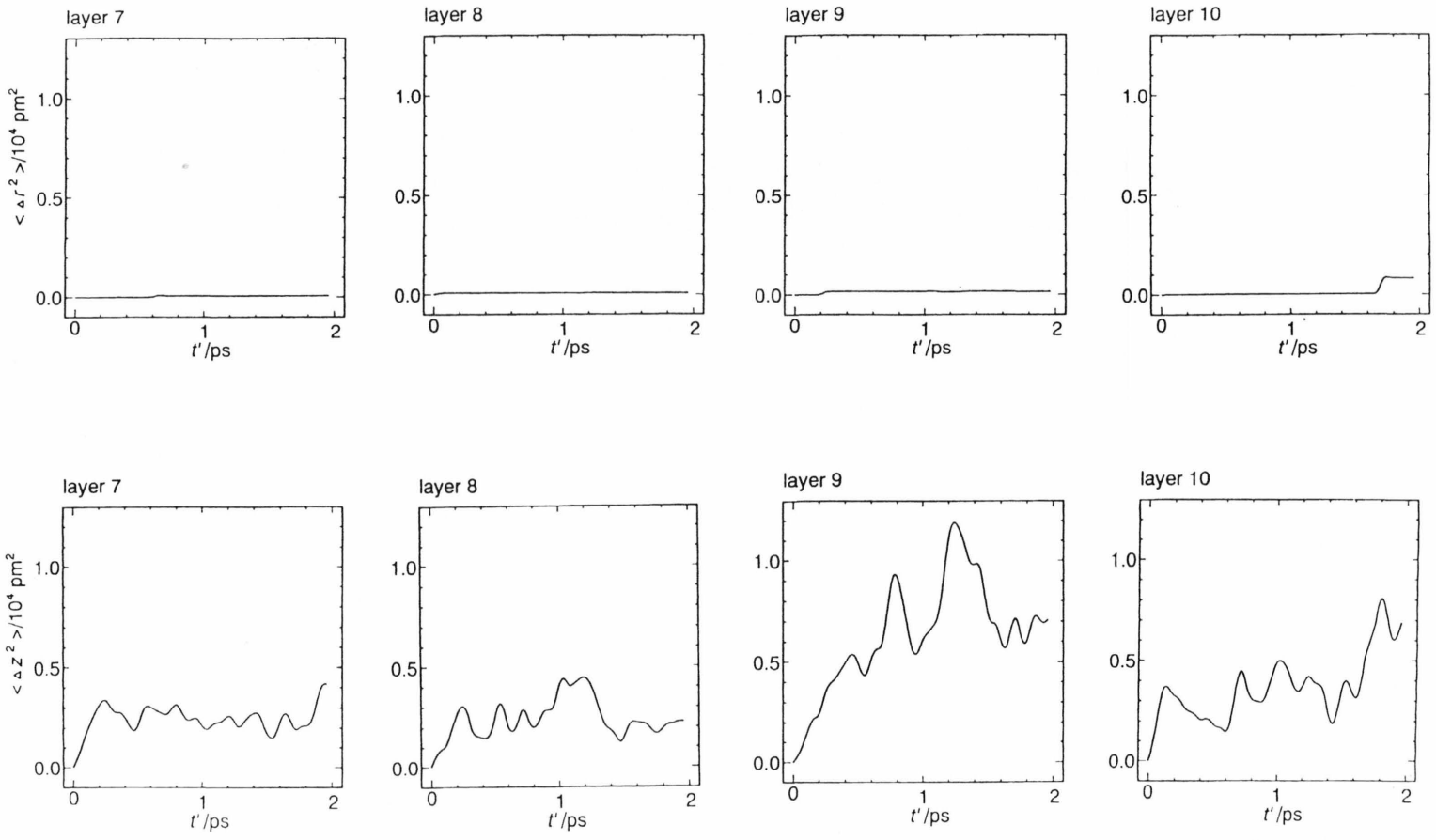

Fig. 12. Mean square displacements in the x-y (upper) and z (lower) directions for (110) for ions present in the indicated layers at $t = 14$ ps.

and -6.426×10^{-19} J/NaCl molecule for the (110) plane, and -5.319 and -5.306×10^{-19} J/molecule for the (110) plane, respectively. Since the repulsive potential is higher for the $Cl^- - Cl^-$ pair than for the $Na^+ - Na^+$ pair, the energy of Na^+ is lower than that of Cl^-. These values also indicate that the (100) plane is stabler than the (110) plane.

The crystal grows faster in the [100] direction (ca. 0.30 layers/ps) than in the [110] direction (0.19 layers/ps), as is qualitatively consistent with the experimental result for KCl [10]. In the [100] direction a "crystallising" ion will come on top of an unlike ion, and, further, the 4 neighbours in the plane of the crystallising ion are unlike ions. On the other hand, in the [110] direction a crystallising ion will sit above the middle of 2 unlike ions, and only neighbours of the crystallising ion in its layer are unlike ions, the other 2 neighbours, though not the nearest, being like ions. Thus, the configuration of the first neighbour ions about every ion in the molten state resembles more that in the (100) face than in the (110) face. This may be the reason why the crystal grows more rapidly on the (100) plane than on the (110) plane. Since the interlayer distances are greater for the (100) planes (ca. 288 pm) than for the (110) planes (ca. 204 pm), the velocity should depend on both the ordering in the layers and the distances between the layers.

In the case of argon, the fcc crystal grows more rapidly on the (111) than on the (100) face [11, 12]. For NaCl a stable (111) surface cannot be created because of the repulsion between like ions. For the soft-sphere model as well as the Lennard-Jones model the structure of the crystal-liquid interface is determined predominantly by the repulsive part of the pair potential [13]. In the present ionic system the attractive part also plays an important role.

Two major mechanisms have been proposed for crystal growth from melts [14]; (1) the interface advances by lateral motion of steps, and (2) the surface advances normal to itself without needing steps. When the driving force is small, the first mechanism dominates, and vice versa. Much work on crystal growth from melts has been performed, (see, e.g. review articles [15, 16]); the above concept [14] seems still to hold.

In the present MD condition, a diffuse interface exists, which suggests the second mechanism. In the present MD simulation even of (100), however, the periodic box was perhaps too small for definite results. Further, the chosen temperature was considerably below melting point. Thus, we do not conclude at present which mechanism operates in reality. MD calculations with larger dimensions may be needed to simulate the mechanism of crystal growth from melt in a real system.

The MD simulations were performed with HITAC M 680 and SX-3/34R computers at the Institute for Molecular Science and a HITAC M 880 computer at National Laboratory for High Energy Physics. The expenses were partly defrayed by the Grant-in-Aid for Scientific Research on Priority Area (Nos. 03243102 and 04227108).

[1] G. H. Gilmer, Atomic-scale Models of Crystal Growth, Handbook of Crystal growth, Vol. 1, ed. D. T. J. Hurle, Elsevier, 1993, p. 585 and the references therein.
[2] M. Tanemura, H. Matsuda, T. Ogawa, N. Ogita, and A. Ueda, J. Non-cryst. Solids **117/118,** 883 (1990).
[3] Landolt-Börnstein Zahlenwerte und Funktionen aus Physik · Chemie · Astronomie · Geophysik · Technik, 6. Auflage 2. Band 1; Teil 1971, 483.
[4] M. P. Tosi and F. G. Fumi, J. Phys. Chem. Solids **25,** 45 (1964).
[5] D. E. Parry, Surface Sci. **49,** 433 (1975); 54, 194 (1976).
[6] D. M. Heyes, M. Barber, and J. H. Clarke, J. Chem. Soc. Faraday Trans. II, **73,** 1485 (1977).
[7] L. V. Woodcock, Chem. Phys. Lett. **10,** 257 (1971). M. P. Tosi and F. G. Fumi, J. Phys. Chem. Solids **25,** 45 (1964).
[8] C. A. MacDonald, A. M. Malvezzi, and F. Spaepen, J. Appl. Phys. **65,** 129 (1989).
[9] E. Burke, J. Q. Broughton, and G. H. Gilmer, J. Chem. Phys. **89,** 1030 (1988).
[10] T. Nakamoto and Y. Ohta, Japan J. Appl. Phys. **15,** 243 (1975).
[11] J. Q. Broughton, G. H. Gilmer, and K. A. Jackson, Phys. Rev. Lett. **49,** 1496 (1982).
[12] E. Burke, J. Q. Broughton and G. H. Gilmer, J. Chem. Phys. **89,** 1030 (1988).
[13] J. N. Cape and L. V. Woodcock, J. Chem. Phys. **73,** 2420 (1980).
[14] J. W. Cahn, Acta Metall. **8,** 554 (1960).
[15] A. R. Ubbelohde, The Molten State of Matter, John Wiley & Sons, New York 1978.
[16] D. T. J. Hurle, ed., Handbook of Crystal Growth 1 a, 1 b, 2 a, 2 b, North-Holland, 1993 and 1994.